



ARTICLE OPEN



Histone lactylation promotes malignant progression by facilitating USP39 expression to target PI3K/AKT/HIF-1 α signal pathway in endometrial carcinoma

Sitian Wei^{1,2}, Jun Zhang^{1,2}, Rong Zhao¹, Rui Shi¹, Lanfen An¹, Zhicheng Yu¹, Qi Zhang¹, Jiarui Zhang¹, Yuwei Yao¹, Haojia Li¹ and Hongbo Wang¹  

© The Author(s) 2024

Histone lactylation has been reported to involve in tumorigenesis and development. However, its biological regulatory mechanism in endometrial carcinoma (EC) is yet to be reported in detail. In the present study, we evaluated the modification levels of global lactylation in EC tissues by immunohistochemistry and western blot, and it was elevated. The non-metabolizable glucose analog 2-deoxy-d-glucose (2-DG) and oxamate treatment could decrease the level of lactylation so as to inhibit the proliferation and migration ability, induce apoptosis significantly, and arrest the cell cycle of EC cells. Mechanically, histone lactylation stimulated USP39 expression to promote tumor progression. Moreover, USP39 activated PI3K/AKT/HIF-1 α signaling pathway via interacting with and stabilizing PGK1 to stimulate glycolysis. The results of present study suggest that histone lactylation plays an important role in the progression of EC by promoting the malignant biological behavior of EC cells, thus providing insights into potential therapeutic strategies for endometrial cancer.

Cell Death Discovery (2024)10:121 ; <https://doi.org/10.1038/s41420-024-01898-4>

INTRODUCTION


Endometrial carcinoma (EC) is one of the most common tumors of the female reproductive system and is the sixth most common cancer in women [1]. EC is a type of malignant epithelial tumor that occurs in the endometrium; however, its specific pathogenesis remains unclear. Recently, the incidence of EC has increased while the age of onset has decreased [1]. Most patients are diagnosed early and have a good prognosis [2]. However, despite the increasing treatment options [3, 4], the outcomes of advanced or poorly differentiated EC and those of particular types of this malignancy are still unsatisfactory [5]. Therefore, there is an urgent need to explore the pathogenesis and effective therapeutic targets for EC in order to improve the prognosis of patients.

Epigenetic modifications play a significant role in the occurrence, development, and metastasis of tumors [6]. These modifications do not change the DNA sequence and are characterized by inheritability and reversibility [7]. Recent studies have resulted in important discoveries regarding post-translational modifications (PTMs) of histone [8]. Histone PTMs change the chromatin structure by regulating DNA-dependent processes, including transcription, replication, and DNA repair, and then regulate gene transcription and expression to play vital roles in maintaining cell homeostasis [9, 10]. These modifications function by changing the contact between nucleosomes or by recruiting nonhistones. At present, many types of histone PTMs have been identified, including acetylation [11], methylation [12], and newly discovered PTMs, such as succinylation [13], glutarylation [14], and

crotonylation [15]. In-depth research has greatly expanded the understanding of the relationships between histone modifications and biological processes [16].

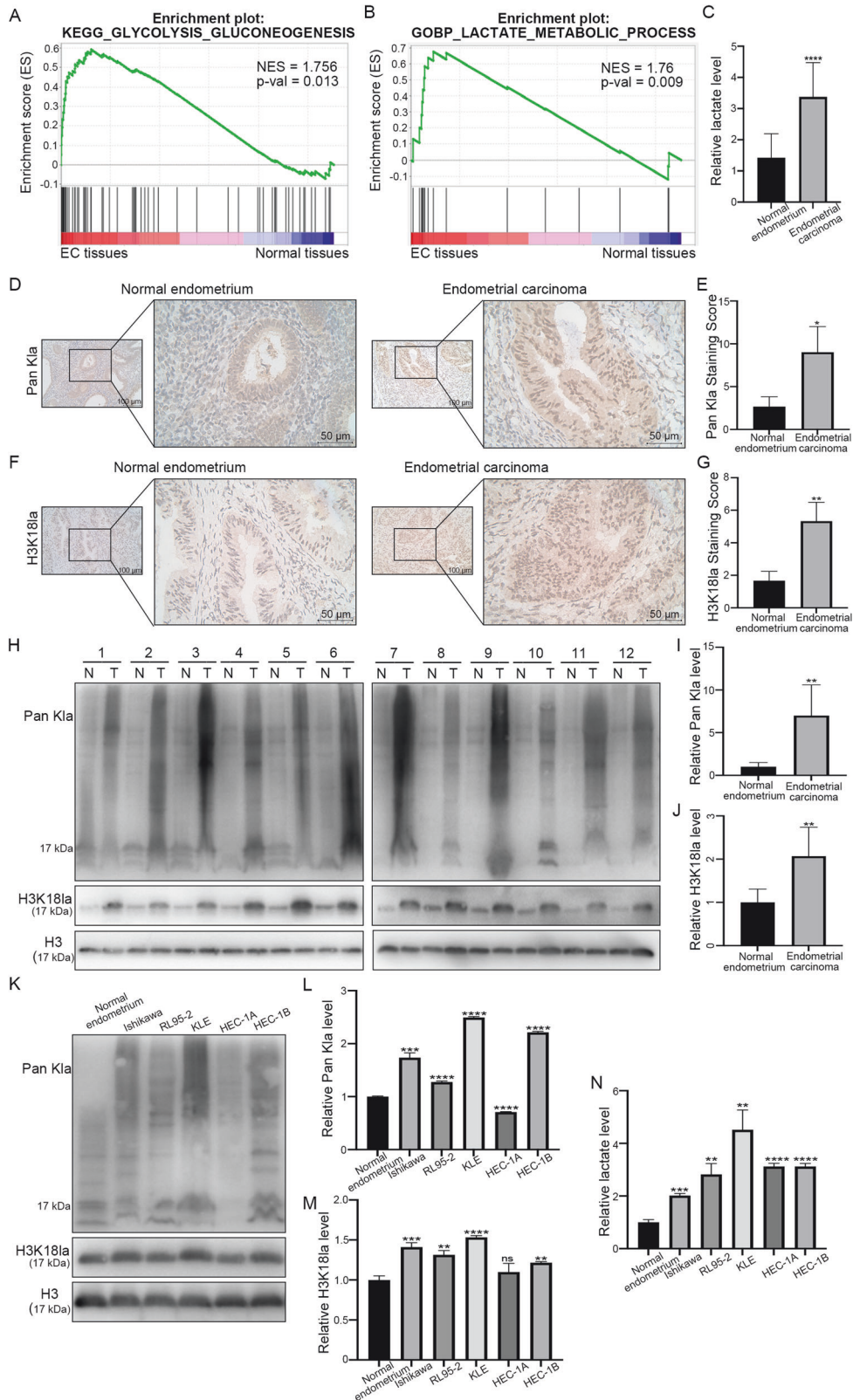
Most tumor cells exhibit active glucose uptake and glycolysis under aerobic conditions [17], known as the Warburg effect [18]. The Warburg effect produces a large amount of lactate, which is widely considered a metabolic byproduct. Since Zhao et al. identified histone lactylation in 2019 [19] as a new epigenetic modification that could directly stimulate gene transcription in the chromatin, an increasing number of studies have found that histone lactylation is involved in the occurrence of tumors, such as ocular melanoma [20] and liver cancer [21], as well as in the development of lung cancer [22] and renal cell carcinoma [23]. Some studies have shown that endometrial cancer tissue contains more lactate than normal endometrial tissue [24, 25]. Therefore, exploring whether histone lactate plays a role in the development of EC may lead to a new strategy for future treatment.

In this study, we found, for the first time, that histone lactylation levels were increased in EC while the suppression of histone lactylation significantly inhibited tumor progression. Mechanistically, histone lactylation promoted the expression of ubiquitin-specific peptidase 39 (USP39), which interacted with, stabilized, and de-ubiquitinated phosphoglycerate kinase 1 (PGK1), thereby activating the PI3K/AKT/HIF-1 α signaling pathway. Our data reveal a novel mechanism of histone lactylation in EC tumorigenesis and provide a theoretical basis for the prevention and treatment of endometrial cancer.

¹Department of Obstetrics and Gynecology, Union Hospital, Tongji Medical College, Huazhong University of Science and Technology, Wuhan, Hubei, PR China. ²These authors contributed equally: Sitian Wei, Jun Zhang.  email: hb_wang1969@sina.com

Received: 24 November 2023 Revised: 23 February 2024 Accepted: 28 February 2024

Published online: 08 March 2024



RESULTS

Histone lactylation levels are elevated in patients with EC

As EC shows active glycolysis and lactate metabolism (Fig. 1A, B), which may lead to a large amount of lactate production as a substrate for histone lactylation, we first determined the lactate

levels in EC and normal endometrial tissues (Fig. 1C). The results showed that the lactate level in the EC tissue was significantly higher than that in normal endometrial tissue. Next, we examined the overall histone lactylation levels in EC. IHC revealed that the global lactylation level in EC tissue was dramatically elevated

Fig. 1 Endometrial carcinoma exhibits increased lactylation levels. **A** KEGG analysis showed EC was active in glycolysis. **B** GO analysis showed EC was enriched in the lactate metabolic process. **C** The lactate levels in EC tissues and normal endometrium were tested. **D** Representative immunohistochemistry (IHC) images of lactylation in EC and adjacent normal tissues. Scale bar: left panel, 100 μm ; right panel, 50 μm . **E** The modification level of lactylation in tumor and adjacent normal tissues from EC patients was detected by IHC. **F** IHC images of H3K181a in EC tissues and adjacent normal tissues. Scale bar: left panel, 100 μm ; right panel, 50 μm . **G** The modification level of H3K181a in tumor and adjacent normal tissues from EC patients was detected by IHC. **H** Lactylation and H3K181a modification levels in EC tissues and adjacent normal tissues were analyzed by western blot. **I, J** Densitometric analysis was performed to quantify and statistically compare lactylation and H3K181a levels in normal and EC tissues. **K** Total lactylation (Pan K1a) and H3K181a modification levels in normal endometrial cells and five EC cell lines were analyzed by western blot. **L, M** The lactylation and H3K181a levels in normal endometrial cells and five EC cell lines were visualized. **N** The lactate levels in normal endometrial cells and five EC cell lines were tested.

compared with that in normal endometrial tissue ($P < 0.05$; Fig. 1D, E). Consistently, western blotting analysis confirmed that the global histone lactylation level in EC tissues was higher than that in adjacent tissues (Fig. 1H, I). Though 28 lactylation sites were identified on core histones, only five antibodies of lactylation sites were developed (H3K181a, H3K271a, H3K141a, H3K91a, and H3K561a) by now. We detected the modification levels of these five sites between EC tissues and normal endometrial tissues and found that H3K181a was changed most significantly (Fig. S1A, B). Therefore, we investigated whether histone lactylation was caused by H3K181a in EC. Similarly, IHC showed that compared with that in normal endometrial tissue, the H3K181a level presented the same trend as the global lactylation level in EC tissue (Fig. 1F, G). Western blotting analysis also confirmed increased H3K181a levels in EC tissues compared with those in adjacent tissues (Fig. 1H, J). Next, we tested the modification levels of total lactylation and H3K181a by western blot and lactate levels by lactate detection assay in normal endometrial cells and five different EC cell lines (Fig. 1K–N). The data suggested that the level of histone lactylation was elevated in EC, which might affect EC progression. Ishikawa and KLE cells were chosen for further studies.

Inhibition of histone lactylation suppresses proliferation and migration, induces apoptosis, and arrests cell cycle progression of EC cells in vitro

To investigate the functional role of histone lactylation in EC cells, we reduced the global intracellular histone lactylation levels in tumor cells. As the endogenous production of lactate is a key determinant of histone lactylation levels [19] and the non-metabolizable glucose analog (2-DG) and oxamate have been reported to be glycolysis inhibitors (Fig. 2A) [26], we adopted these compounds to attenuate lactate production and histone lactylation. The CCK-8 assay was used to determine the half-maximal inhibitory concentration (IC₅₀) values of 2-DG and oxamate against Ishikawa and KLE cells (Fig. S2A, B). The data showed that the IC₅₀ values of 2-DG and oxamate against Ishikawa cells were 10.22 and 17.84 mM, respectively, and those against KLE were 9.33 and 16.25 mM, respectively. Accordingly, we established corresponding concentration gradients and found that with the increases in 2-DG treatment concentrations, the relative intracellular pyruvate and lactate levels in both EC cell lines showed significant dose-dependent decreases (Fig. S2C, Fig. 2B). The same lactate content tendency was observed when treated with oxamate (Fig. 2C). Global lactylation and H3K181a levels significantly decreased in EC cells in a dose-dependent manner (Fig. 2D, E). Meanwhile, the CCK-8 assay and colony formation assays suggested that the reduction in histone lactylation effectively inhibited the proliferation of EC cells (Fig. 2F–I). Transwell assays showed that the migratory ability of EC cells was reduced after 2-DG or oxamate treatment (Fig. S3A, B). Moreover, we observed an abrupt increase in the proportion of apoptotic cells in the 2-DG-treated group compared with that in the control group (Fig. S3C). Next, we performed FACS of Ishikawa and KLE cells for cell cycle analysis. The proportions of cells in the G₀/G₁ phase sharply increased, whereas those in the S phase dramatically decreased after treatment with 2-DG (Fig. S3D).

In summary, these findings confirm that suppressing histone lactylation can efficiently inhibit the proliferation and migration, induce apoptosis, and arrest cell cycle progression from the G₀/G₁ to the S phase in EC cells.

H3K181a regulates the expression of USP39 in EC cells

To investigate the regulatory role of histone lactylation in gene expression, we first performed RNA sequencing (RNA-seq) of Ishikawa cells with and without 2-DG treatment (Fig. 3A). The differentially expressed genes were analyzed by GO function enrichment and KEGG pathway enrichment, and the enrichment results were visualized to understand the biological functions of the K1a-mediated molecular mechanism (Fig. S4A, B). When analyzing the RNA-seq data of the transcriptome (Table S2), we focused on ubiquitin-specific peptidase 39 (USP39), which had a significantly decreased mRNA level in 2-DG-treated cells (Fig. 3B) and has been reported to act as an oncogene in several tumors. Therefore, USP39 might be the potential downstream target of histone lactylation. To confirm that H3K181a regulated the expression of USP39, we performed ChIP-qPCR analysis, which showed that H3K181a was enriched in the USP39 promoter region (Fig. 3C, D). This enrichment was efficiently reduced by the glycolysis inhibitor 2-DG (Fig. 3C, D). To further examine whether histone could bind to the USP39 promoter active region in vitro, an EMSA was conducted. According to ChIP-PCR results, we designed biotin-labeled probes based on binding sites c (GGAGCAGCCCTGAAAGTTTA) and d (TAAGCCTTGATGCCA-CACCA). After the addition of Ishikawa or KLE histone, the slow shift band appeared (Fig. 3E). These results indicated that histone indeed bound to the predicted promoter active region binding site of USP39 in vitro. As expected, the mRNA (Fig. 3F) and protein (Fig. 3G) expression levels of USP39 dramatically decreased after 2-DG treatment. Overall, these data suggest that H3K181a regulates USP39 expression in EC cells.

USP39 is involved in the progression of EC

As USP39 can be directly regulated by H3K181a, we next explored USP39 function in EC. First, we performed data mining and analyzed 575 EC cases from The Cancer Genome Atlas (TCGA) database. The expression of USP39 in non-tumor samples ($n = 23$) was much lower than that in EC tumor samples ($n = 552$) ($P < 0.05$; Fig. 4A), and higher expression of USP39 was positively correlated with the clinical grade and FIGO stage of EC ($P < 0.05$; Fig. S5A, B). Moreover, a high USP39 level was associated with a poorer prognosis of patients ($P < 0.05$; Fig. S5C). As Fig. S5D showed, patients with copy-number-high (CN high) had the highest USP39 expression, compared with the risk score of patients with polymerase epsilon (POLE) ultramutated, microsatellite-unstable (MSI), or copy-number-low (CN low). The six pairs of tumor specimens and their corresponding adjacent normal tissues from patients with EC were analyzed by western blot. The results indicated that the expression level of USP39 in EC tumor tissue was dramatically higher than that in the normal endometrium (Fig. 4B). Next, EC cell lines were transfected with si-USP39 to downregulate the expression of USP39. The mRNA and protein expression levels of USP39 were significantly decreased in

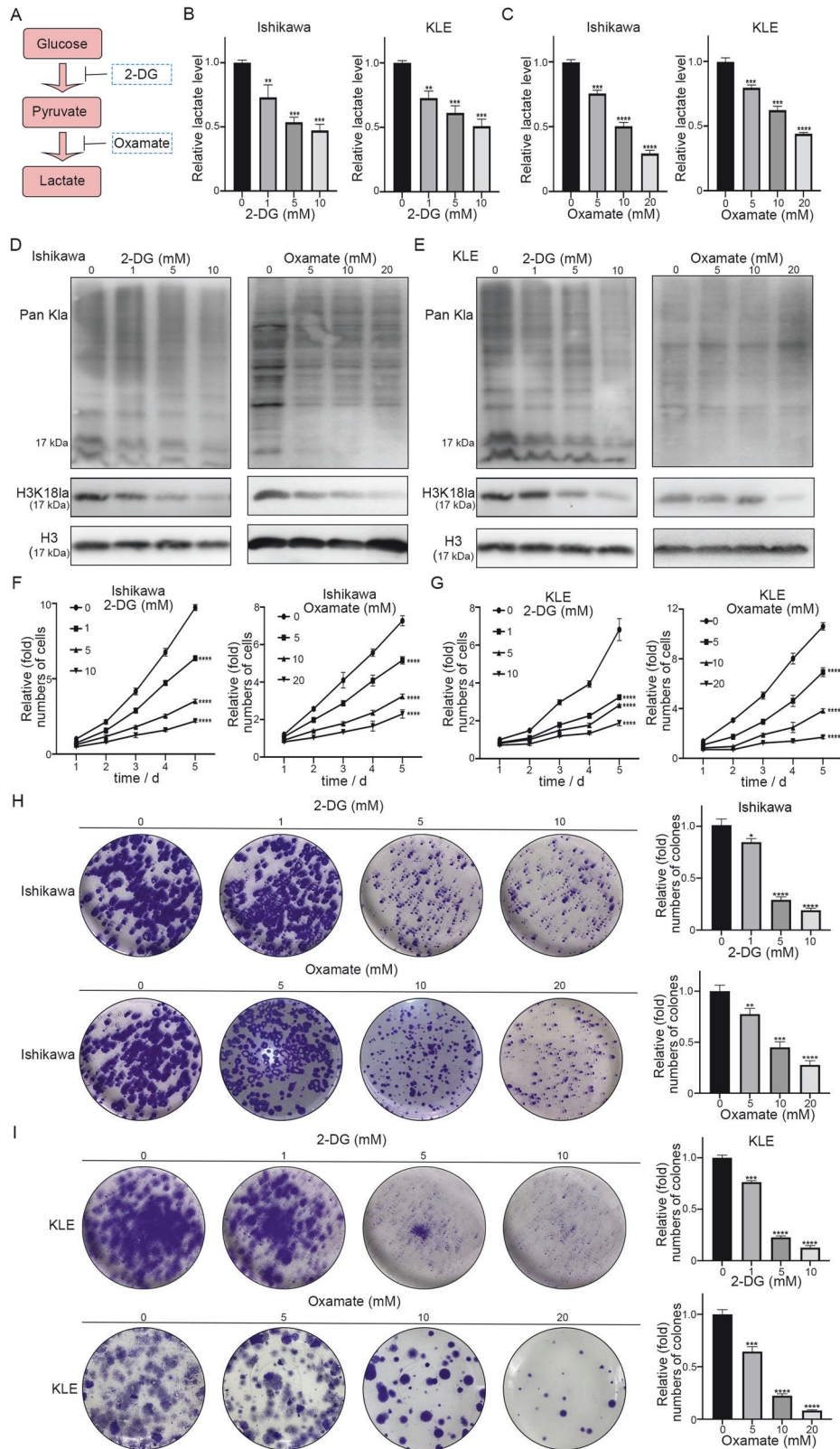


Fig. 2 2-DG and oxamate reduces lactylation levels, and inhibition of histone lactylation suppresses EC proliferation. **A** Schematic diagram of target for inhibiting histone lactylation. **B, C** Intracellular lactate levels were measured from Ishikawa and KLE cells cultured in different concentrations of 2-DG or oxamate. **D, E** Histone lactylation and H3K18la levels were detected in Ishikawa and KLE cells cultured in different concentrations of 2-DG or oxamate by western blot. **F, G** Cell proliferation was detected by CCK8 assay following 2-DG or oxamate treatment in EC cells. **H, I** Cell proliferation was detected by colony formation assay following 2-DG or oxamate treatment in EC cells.

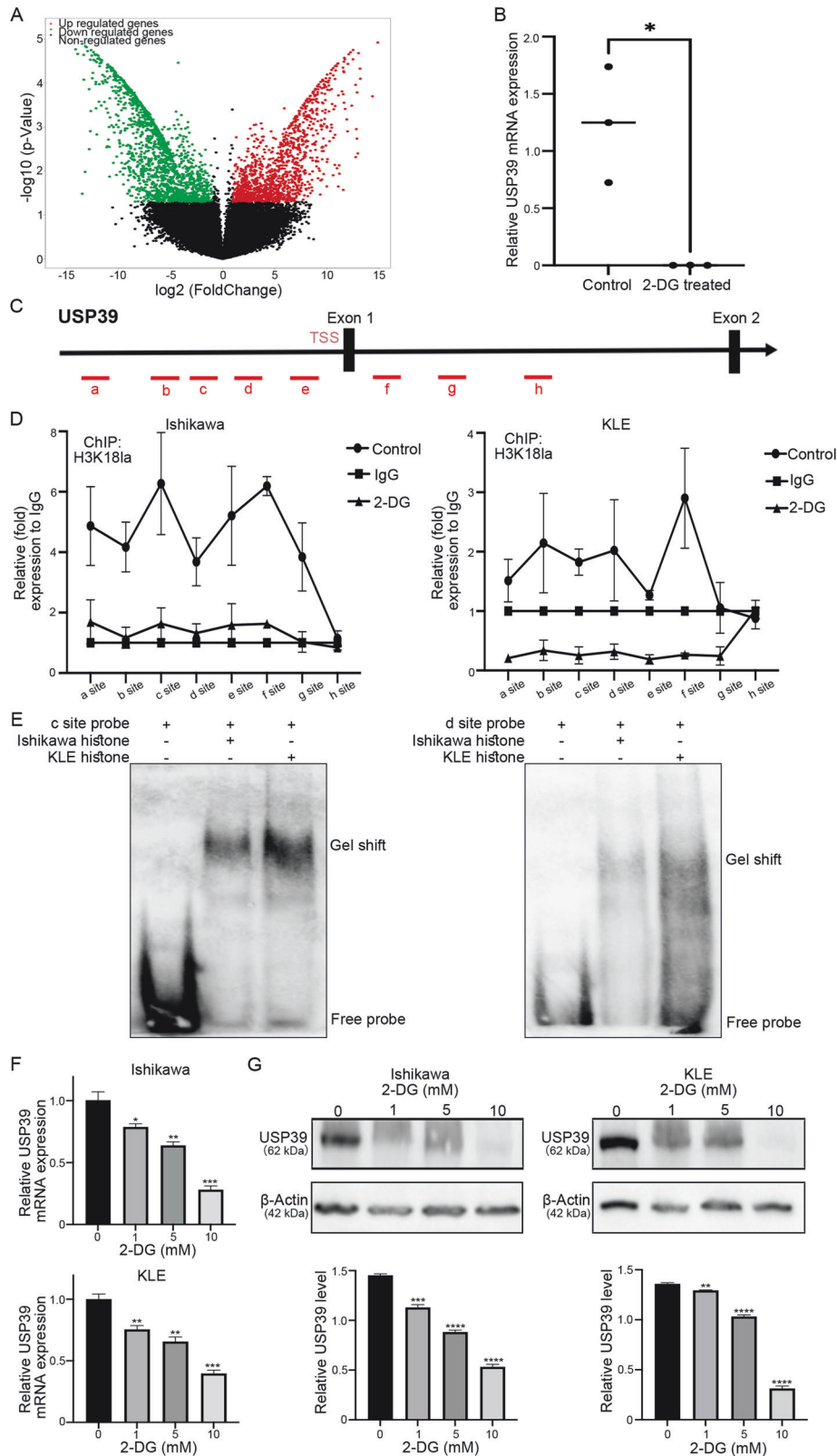


Fig. 3 Histone lactylation regulated the expression of USP39. **A** The volcano plot showed differentially expressed genes from the RNA-seq results of Ishikawa cells treated with 2-DG or not. **B** The relative expression of USP39 mRNA from the RNA-seq results of Ishikawa cells treated with 2-DG or not. **C** Distribution of H3K181a sites relative to the translation start site (TSS) of USP39. **D** The ChIP-qPCR analysis about H3K181a enrichment in the USP39 promoter region. H3K181a enriched around the USP39 TSS, and this enrichment was reduced efficiently by 2-DG. **E** EMSA was performed to analyze the binding of histone to the USP39 promoter fragment. **F** qRT-PCR was performed to test USP39 mRNA expression in Ishikawa and KLE cells after being treated with different concentrations of 2-DG. **G** Western blot was performed to test the USP39 protein level in Ishikawa and KLE cells after being treated with varying concentrations of 2-DG.

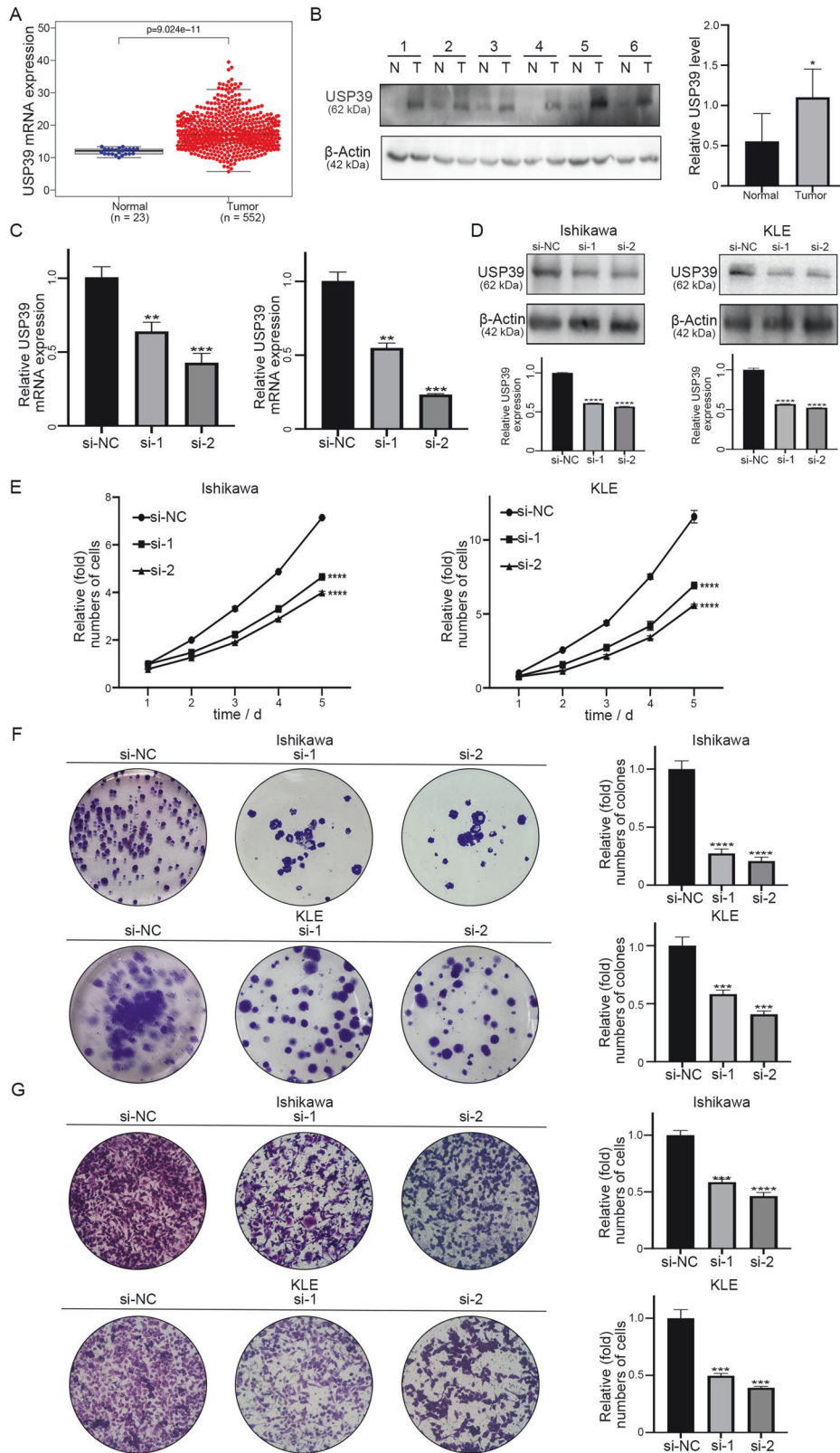


Fig. 4 Knockdown of USP39 suppresses cell proliferation and migration of EC cells *in vitro*. **A** The mRNA expression of USP39 in endometrial tumor tissues and normal endometrial tissues was analyzed based on TCGA databases. **B** USP39 protein expression in EC tissues and adjacent normal tissues was analyzed by western blot. **C** The knockdown efficiency of si-USP39 was detected by qRT-PCR in Ishikawa and KLE cells. **D** The knockdown efficiency of si-USP39 for following experiments was validated by western blot. **E, F** Cell proliferation was detected by CCK8 and colony formation assay following USP39 knockdown in EC cells. **G** Cell migration ability was determined by transwell assay following USP39 knockdown in EC cells.

Ishikawa and KLE cells compared with those in the corresponding negative control (Fig. 4C, D). CCK-8 and colony formation assays suggested that the downregulation of USP39 inhibited the proliferation of tumor cells (Fig. 4E, F). In addition, Transwell assays indicated that lower levels of USP39 were associated with a poor migration ability of the cells (Fig. 4G).

We then examined whether the EC tumor suppression effect of the treatment with the histone lactylation inhibitor 2-DG could be reversed by increased USP39 levels. After USP39 was successfully upregulated (Fig. 5A, B), we performed CCK-8 (Fig. 5C) and EdU assays (Fig. 5D), which showed that the growth of EC cells was markedly increased compared with that of control cells. In addition, we observed that the migration ability of EC tumor cells was enhanced after USP39 overexpression, as measured by Transwell assays (Fig. 5E). Moreover, after overexpression of USP39 in EC cells, the 2-DG-induced suppression of USP39 mRNA and protein expression was reversed (Fig. 5A, B), and the anticancer effect of 2-DG was weakened based on the cell growth (Fig. 5C, D) and migration (Fig. 5E). Together, these data suggest that USP39 acts as an oncogene in EC.

Histone lactylation and USP39 promote EC development, and USP39 overexpression reverses the suppression of tumor growth by 2-DG in vivo

To verify the effect of histone lactylation and USP39 on endometrial cancer, we established an EC xenograft tumor model in nude mice and evaluated the outcomes *in vivo*. Ishikawa cells pretreated with 2-DG and/or an USP39 vector were subcutaneously injected into nude mice. The tumor size was measured every 5 days until the mice were sacrificed on day 25. As expected, the tumor volume in the group with reduced histone lactylation was significantly inhibited (Fig. 6A, B), and the weight was dramatically lower than that in the control group (Fig. 6C). HE staining showed that Ishikawa cells grew well (Fig. S6A), and IHC showed that the modification levels of Pan K1a and H3K181a significantly decreased after 2-DG treatment (Fig. 6D, E). In addition, overexpression of USP39 accelerated the tumor growth and reversed the 2-DG-caused tumor inhibition (Fig. 6A–C). The IHC results suggested that after 2-DG treatment, the expression level of the USP39 protein in tumors decreased, while the upregulation of USP39 reversed this decrease (Fig. 6F). Subsequently, a tail vein injection-induced EC lung metastasis mouse model was used to evaluate the effect of histone lactylation on EC cell metastasis. As shown in Fig. 6G, no obvious metastatic foci were observed in the lungs after 2-DG treatment, while overexpression of USP39 led to a significantly increased volume of metastatic foci, which could be inhibited by 2-DG treatment. The HE staining results confirmed this trend (Fig. S6B). These data demonstrate that 2-DG can inhibit histone lactylation, thereby weakening EC growth and metastasis, and USP39 overexpression can reverse this tumor-suppressive effect.

Histone lactylation and USP39 accelerate glycolysis by activating the PI3K/AKT/HIF-1 α signaling pathway in EC

As KEGG pathway enrichment analysis suggested that the PI3K-AKT and HIF-1 signaling pathways were two of the most significant pathways enriched by USP39, we investigated whether histone lactylation and USP39 could promote the expression of PI3K and its critical downstream protein, HIF-1 α , as well as glycolysis, *in vitro*. The treatment with 2-DG significantly inhibited the PI3K, phospho-PI3K (p-PI3K), AKT, phospho-AKT (p-AKT), and HIF-1 α levels in EC cells (Fig. 7A, B). USP39 efficiently induced the phosphorylation of PI3K and AKT and increased HIF-1 α expression in EC cells (Fig. 7A, B). In addition, USP39 reversed the 2-DG-induced decreases in the levels of p-PI3K, p-AKT, and HIF-1 α (Fig. 7A, B). The lactate levels in Ishikawa and KLE cells were consistent with these trends (Fig. 7C), while the intracellular glucose content showed the opposite trend (Fig. 7D). Moreover, we found that the

ATP content decreased with 2-DG treatment and was relatively increased by reversing the USP39 level (Fig. 7E). In addition, we demonstrated by western blotting that the expression of the glycolysis-related proteins GLUT-1, HK2, LDHA, MCT-1, and MCT-4 was decreased by 2-DG treatment and was enhanced by USP39 vectors (Fig. 7F). Next, we used LY294002, a typical PI3K inhibitor, to treat Ishikawa and KLE cells transfected with USP39-expressing vectors. LY294002 effectively reduced the levels of PI3K, p-PI3K, AKT, p-AKT, and HIF-1 α , which were elevated by USP39 (Fig. 7G). Collectively, these results indicate that histone lactylation and USP39 promote PI3K/AKT- and HIF-1 α -mediated glycolysis in EC cells.

USP39 stabilizes PGK1 by de-ubiquitination to regulate the PI3K/AKT pathway

Next, we explored the mechanism of PI3K/AKT pathway regulation by USP39 via analysis of proteins that interacted with USP39. Using Co-IP, followed by mass spectrometry (MS), we identified a number of proteins that could interact with USP39. As shown in Fig. S7A, which presents the MS data, we paid particular attention to candidates that were detected in the USP39 group but not detected in the IgG group. Phosphoglycerate kinase 1 (PGK1), the first ATP-generating enzyme in the glycolytic pathway, has been reported to activate the PI3K/AKT pathway and was chosen for further binding validation by investigating whether endogenous USP39 and PGK1 could interact with each other. A reciprocal IP experiment was conducted in which an endogenous PGK1 protein was co-immunoprecipitated with USP39 (Fig. 8A), indicating that these two proteins could interact endogenously. This result was confirmed by a reciprocal Co-IP assay (Fig. 8B). Moreover, USP39 downregulation resulted in a decrease in the PGK1 protein levels in EC cells (Fig. 8C). To exclude the possibility that the downregulation of the PGK1 protein occurred at the transcriptional level, qRT-PCR was performed to measure the PGK1 and USP39 mRNA levels. In contrast to the significant decrease in the USP39 mRNA level, the PGK1 mRNA level was similar to that in the control cells (Fig. 8D), suggesting that the effect of USP39 on PGK1 was not mediated at the transcriptional level. As USP39 is a de-ubiquitinating enzyme, we explored whether the USP39 de-ubiquitination activity stabilized the PGK1 protein. First, we hypothesized that USP39 extended the half-life of PGK1. PGK1 levels were monitored after treatment with the protein inhibitor cycloheximide (CHX). In the absence of *de novo* protein synthesis, the half-life of endogenous PGK1 was shorter in USP39-depleted cells than in control cells (Fig. 8E). In addition, the decrease in the PGK1 protein level was reversed by the treatment of Ishikawa and KLE cells with the proteasome inhibitor mg132 (Fig. 8F). HA-ubiquitin and His-PGK1 constructs were co-expressed, with or without Flag-USP39, in Ishikawa and KLE cells. Ectopic expression of Flag-USP39 markedly promoted PGK1 de-ubiquitination (Fig. 8G). Conversely, the USP39 knockdown increased PGK1 ubiquitination in EC cells (Fig. 8H), indicating that USP39 is responsible for PGK1 deubiquitination. Taken together, these data demonstrate that USP39 can stabilize the PGK1 protein by deubiquitination in a proteasome-dependent manner in EC cells.

DISCUSSION

Epigenetic modifications play a crucial role in the occurrence, development, and metastasis of tumors. The study of histone modifications is expected to further elucidate the mechanisms of tumor progression and metastasis and provide a reliable basis for the research and development of antitumor drugs [27]. Small molecules involved in cell metabolism participate in a variety of epigenetic modifications [28]. In particular, acetyl-CoA [29], S-adenosyl methionine [30], and succinate [31] participate as substrates or cofactors in PTM processes such as acetylation, methylation, and succinylation, respectively. Therefore,

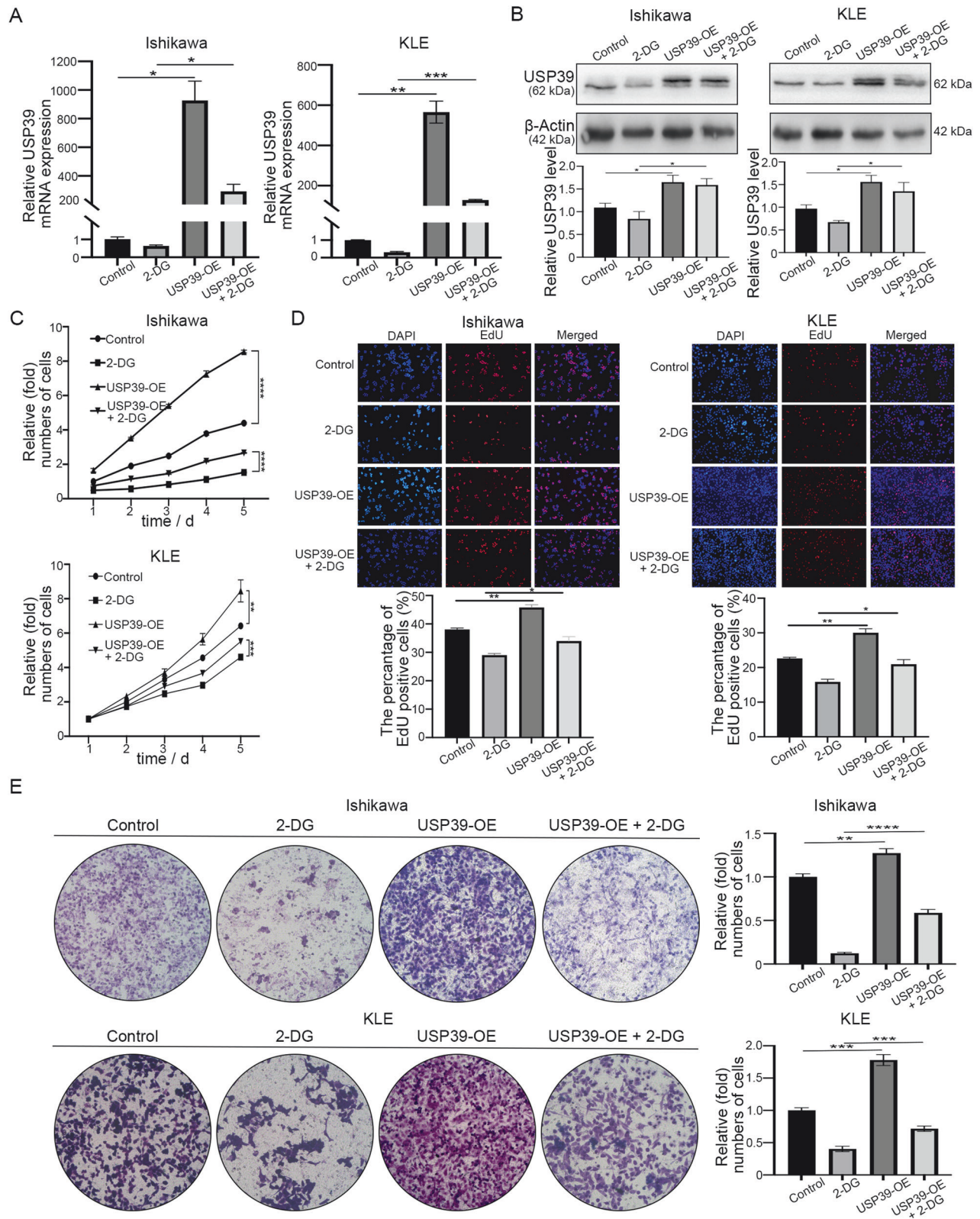


Fig. 5 USP39 rescues the reduction of lactylation caused by 2-DG. **A** qRT-PCR showed that USP39 was silenced after 2-DG treatment, upregulated after overexpressing USP39, and could be rescued in EC cells. **B** Western blot showed the USP39 protein level after cocultured with 2-DG and/or USP39 vector. **C** Cell proliferation was assessed by CCK8 assay after down- and/or over-expression of USP39. **D** Images and statistical analysis of cells in the EdU assay were performed using Ishikawa and KLE cells with or without USP39 knockdown. **E** Migration of EC cells with or without USP39 knockdown was analyzed by transwell assay.

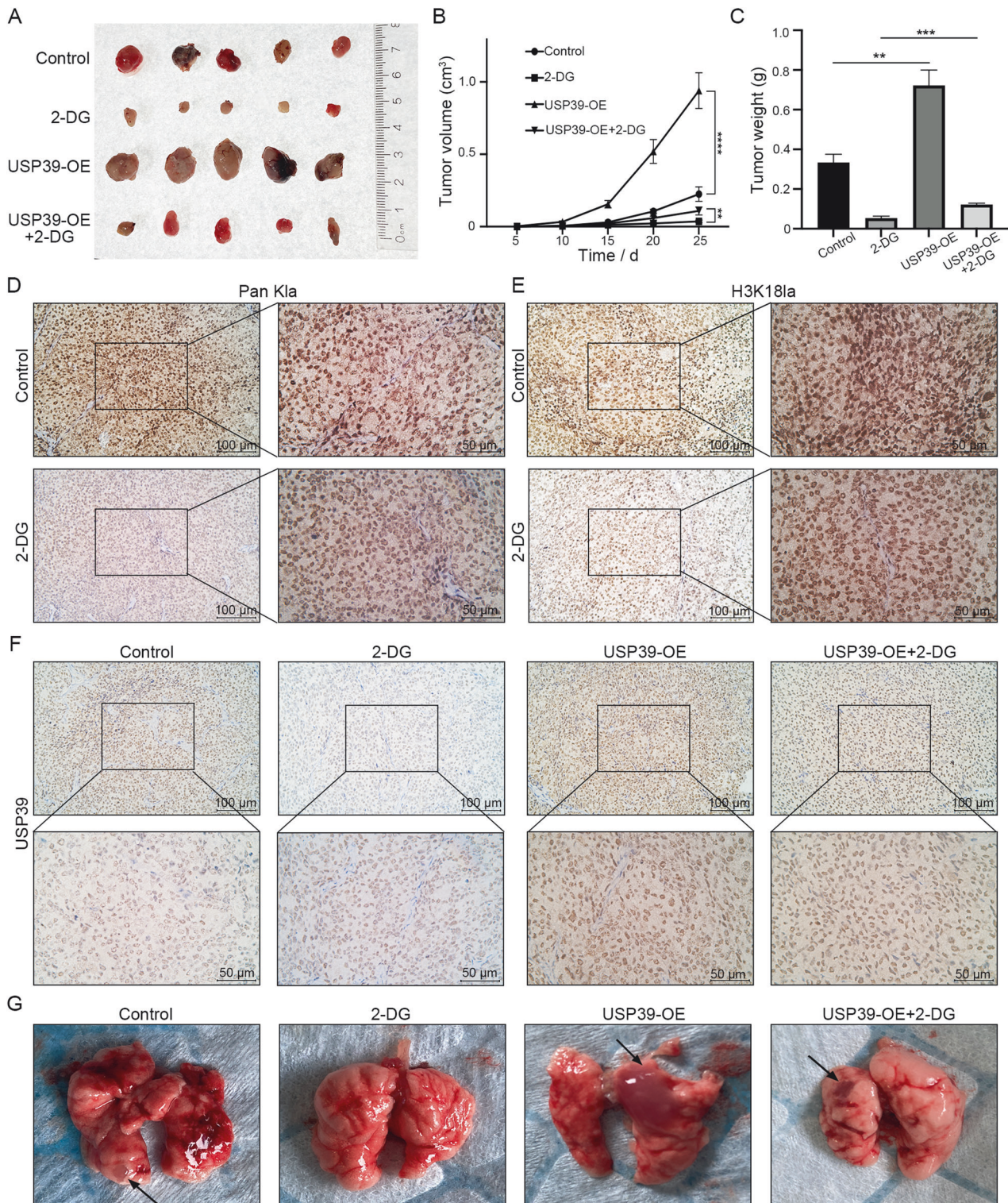


Fig. 6 Histone lactylation and USP39 promote EC proliferation and metastasis in vivo. **A** Images of xenograft tumors from BALB/c-nude mice 25 days after the subcutaneous injection of Ishikawa cells. **B** Tumor volume was measured every 5 days and calculated according to the formula: $(\text{length} \times \text{width}^2)/2$. **C** Tumor weight of nude mice was assessed on day 25. **D** Immunohistochemistry (IHC) for lactylation modification levels in xenograft tumors. Scale bar: left panel, 100 μm ; right panel, 50 μm . **E** IHC for H3K18la levels in xenograft tumors. Scale bar: left panel, 100 μm ; right panel, 50 μm . **F** IHC for USP39 expression in xenograft tumors. Scale bar: upper panel, 100 μm ; lower panel, 50 μm . **G** Metastatic foci in the lung sections were marked by arrows.

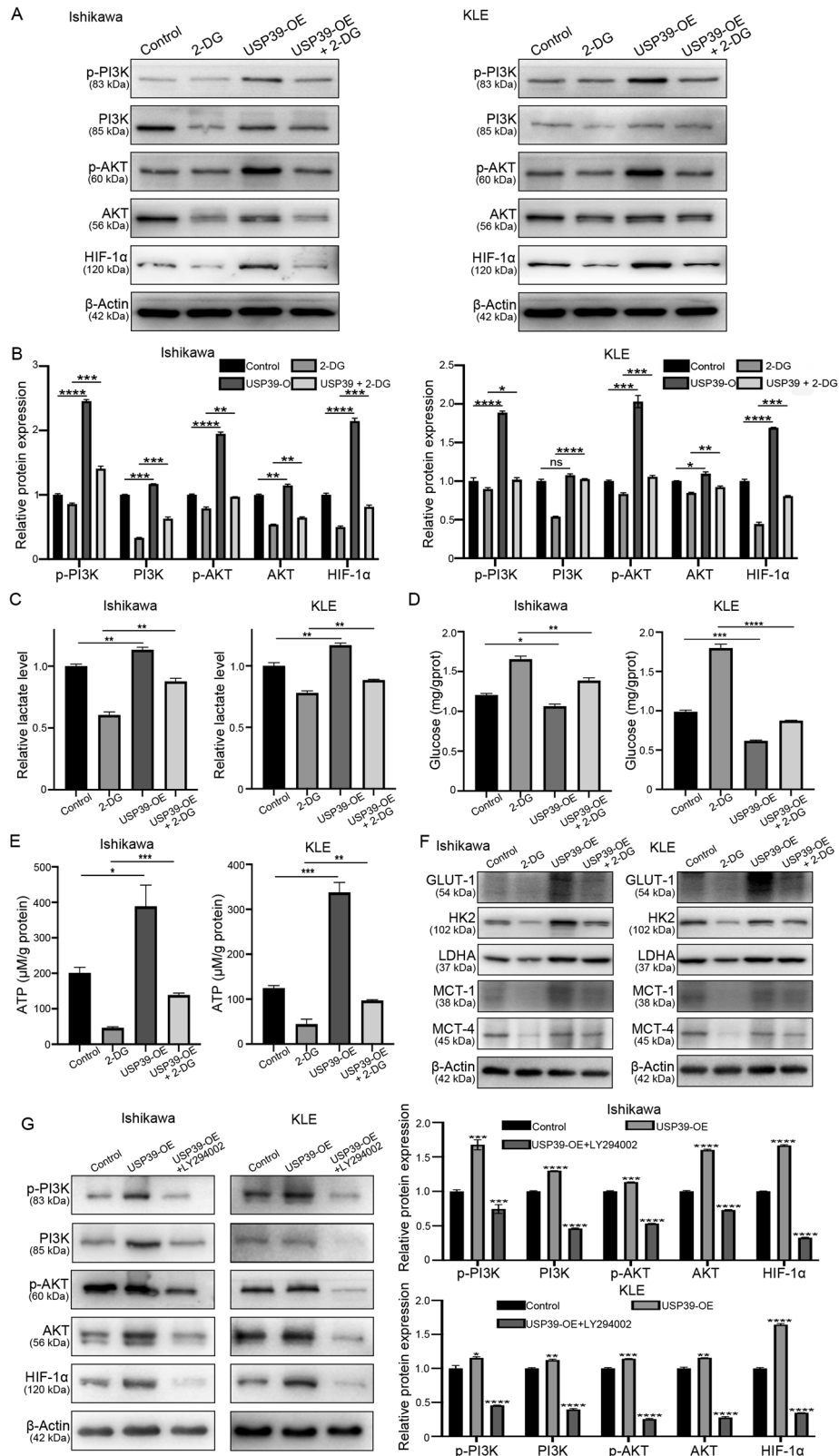


Fig. 7 Histone lactylation and USP39 enhance glycolysis via activating PI3K/AKT/HIF-1 α signaling pathway. **A** The protein levels of PI3K, p-PI3K, AKT, p-AKT, and HIF-1 α in Ishikawa and KLE cells were detected by western blot after being treated with varying conditions. **B** The quantitative analysis of the protein levels of PI3K, p-PI3K, AKT, p-AKT, and HIF-1 α . **C** Measurement of intracellular lactate levels in cells treated in varying conditions. **D** Measurement of intracellular glucose levels in cells treated in varying conditions. **E** Measurement of intracellular ATP levels in cells treated in varying conditions. **F** The expression levels of five glycolysis-related proteins when treated with 2-DG and/or USP39 by western blot. **G** The Protein levels of PI3K, p-PI3K, AKT, p-AKT, and HIF-1 α after being treated with LY294002 by western blot.

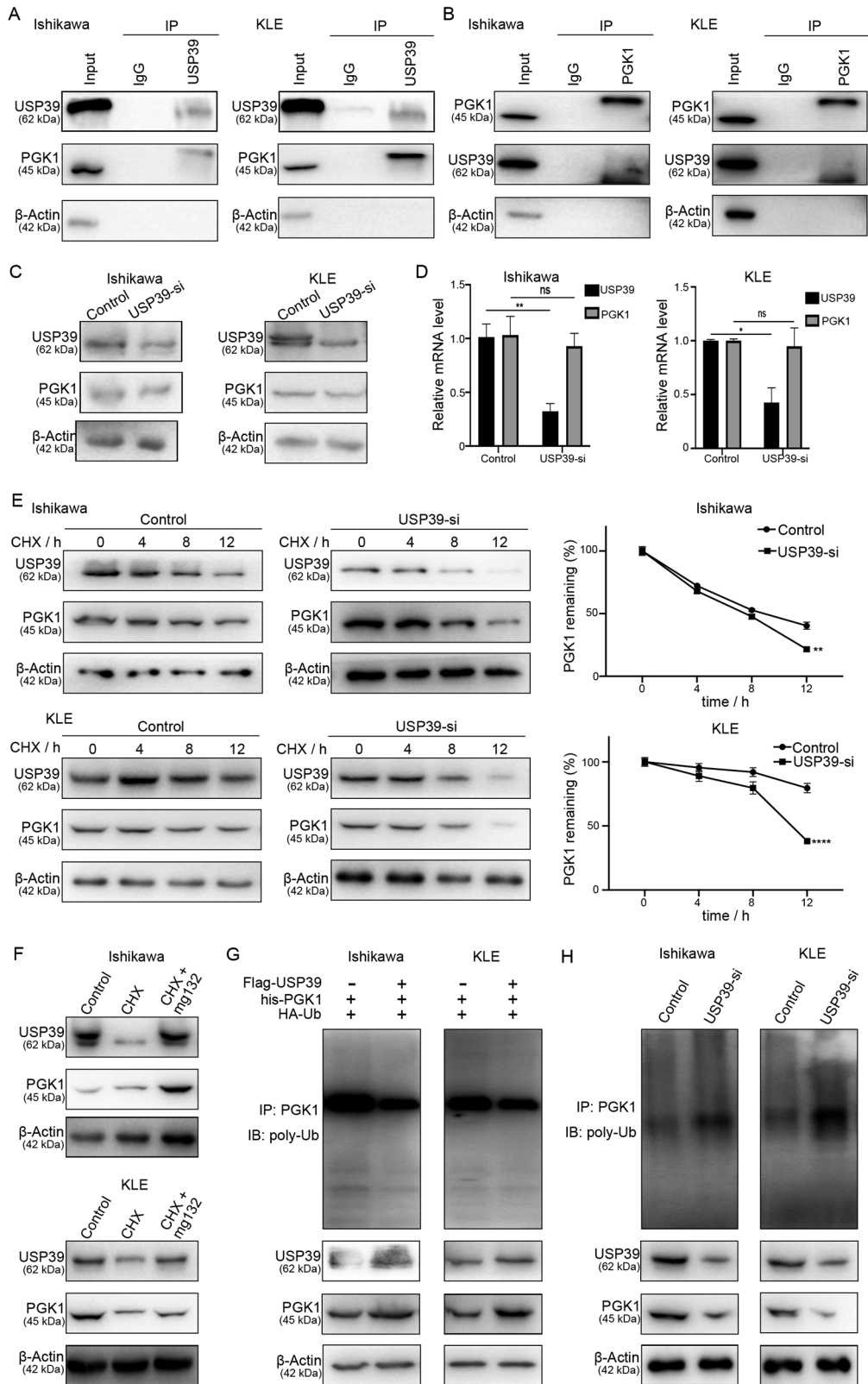


Fig. 8 USP39 interacts with PGK1 and stabilizes PGK1 by de-ubiquitination. **A** The immunoprecipitates were blotted with anti-USP39 in Ishikawa and KLE cells. **B** The immunoprecipitates were blotted with anti-PGK1 in Ishikawa and KLE cells. **C** EC cells were prepared for western blotting analysis with anti-USP39 and anti-PGK1 after being transfected with USP39 siRNA. **D** qRT-PCR analysis of the mRNA levels of USP39 and PGK1 in USP39 knocked down cells. **E** The PGK1 level and degradation rate after cycloheximide (CHX) treatment. **F** Western blot was performed with cells treated with mg132. **G** The ubiquitinated forms of PGK1 were analyzed by western blotting analysis with the condition with HA-Ub and his-PGK1 along with Flag-USP39 constructs were co-transfected into Ishikawa and KLE cells. **H** The ubiquitinated forms of PGK1 were analyzed by western blotting analysis after USP39 siRNA was transfected into Ishikawa and KLE cells.

metabolites play a prevalent and essential role in the epigenetic modification of tumors. As the Warburg effect is one of the hallmarks of cancer, even under aerobic conditions, cancer cells tend to produce lactate via anaerobic glycolysis to generate energy, thus producing more lactate than normal cells at a given time [32]. Used as a metabolic byproduct, lactate has been discovered to alter histones by the addition of the lactyl group, which is described as histone lactylation. Histone lactylation is caused by lactate, and the process is sensitive to lactate levels. Studies have shown that under hypoxia or bacterial infection, intracellular glucose is not completely oxidized, and the produced metabolite lactate stimulates the histone lactylation modification and activates downstream gene expression [33–35]. With regard to the broader roles of this modification, lactate is generated by cells under both physiological conditions and disease states, such as cancer. Histone lactylation participates in cellular communication and regulates the immune system [36], links cellular metabolism to gene regulation, and may have numerous implications for human health. Owing to the active glycolysis and lactate metabolism processes in EC, we suspect that histone lactylation in EC is likely to be abnormal. Thus, exploration of the potential role of histone lactylation in the occurrence and development of EC tumors is of great significance.

MS analysis identified 26 histone K1a sites on core histones, including H3K9, H3K18, and H3K28, from human MCF-7 cells [19]. Most studies have focused on H3K18, which may be due to the imperfect development of corresponding antibodies to other sites. Gene Ontology analysis has shown that H3K18la-specific genes were enriched in biological pathways unrelated to inflammation, including the induction of arginase 1 expression [19].

In this study, we first demonstrated by IHC and western blotting that global lactylation was increased in EC. In vitro experiments showed that glycolysis inhibitors, 2-DG and oxamate, reduced the global lactylation levels and those at a selected K1a site, H3K18la, in a concentration-dependent manner. It was also found that after treatment with 2-DG and oxamate, the proliferation and migration of EC cells were significantly inhibited, while the rate of apoptosis was dramatically increased, and the cell cycle was effectively blocked. In addition, in vivo studies using mice models showed that decreasing lactylation significantly reduced the volume and weight of tumors and suppressed metastasis. These data confirm the fundamental role of histone lactylation as a new target for the prevention of EC tumor development.

To explore the potential downstream targets of histone lactylation, we performed RNA-seq to compare the mRNA levels between control and EC cells treated with 2-DG. Consequently, we selected genes that were highly expressed in EC tumor cells and whose mRNA levels were significantly reduced in 2-DG-treated cells. Among multiple candidate genes, we focused on USP39, which has been reported to act as a carcinogen in various tumors. Deubiquitinases are a large protease superfamily [37], among which the ubiquitin-specific protease family (also known as ubiquitin-specific processing enzymes) has the largest number of members and the most diverse structure [38]. This family contains two short conserved fragments, lysine and histidine boxes. The sequence contains a catalytic triad of cysteine, histidine, and aspartic acid or asparagine residues, which can remove ubiquitin molecules from large proteins [39]. Thus, USP15 is related to the COP9 signalosome complex and is involved in the regulation of a variety of signaling pathways [40]. In the base excision repair pathway, USP47 deubiquitinates and stabilizes monoubiquitinated DNA polymerase β [41]. USP30 can remove ubiquitin tags and participate in the regulation of mitochondrial morphology in cells, thus inhibiting mitochondrial autophagy [42]. Previous studies have shown that USP39 is significantly involved in the occurrence and development of cancer. In particular, USP39 de-ubiquitinates and stabilizes CHK2 to regulate the DNA damage response and chemical radiation resistance [43],

de-ubiquitinates and stabilizes the SP1 protein to promote hepatocellular carcinoma progression [44], and inhibits VEGF-A165b-selective splicing by regulating SRSF1 and SRPK1 to promote malignant proliferation and angiogenesis of renal cell carcinoma [45].

In this study, we further explored whether H3K18la could regulate the expression of USP39. We then performed ChIP-qPCR and EMSA analysis, and the results showed that H3K18la was enriched in the USP39 promoter region, and this enrichment was efficiently reduced by 2-DG. Next, we confirmed that USP39 was upregulated in EC by analyzing online databases and clinical samples. Using CCK8, EdU, and colony formation assays, as well as in vivo trials, USP39 was shown to promote EC proliferation and migration. As the PI3K/AKT pathway is common in various cancers [46], we verified whether USP39 could stimulate PI3K/AKT/HIF-1 α signaling to accelerate glycolysis.

As USP39 is a deubiquitinase, we investigated its interacting proteins. Based on the MS results, followed by Co-IP, we focused on PGK1, the first ATP-generating enzyme in the glycolytic pathway and a HIF-1-targeted gene [47–49], which has been reported to activate the PI3K/AKT pathway [50]. A reciprocal IP experiment and a reciprocal assay confirmed that PGK1 and USP39 interacted with each other. In addition, USP39 deubiquitinated and stabilized PGK1. Most importantly, USP39 regulated the PI3K/AKT/HIF-1 α signaling pathway via interaction with PGK1.

Our study has some limitations. Only twelve pairs of EC and normal tissue samples were available, and the only pathological type was endometrioid adenocarcinoma. Expanding the number of tissue samples and pathological types of EC and following up on prognosis should be considered. Finding compounds that can directly target lactylation sites could help elucidate the mechanism of histone lactylation in EC. Further experiments were required to establish the role of H3K18la in the transcriptional activation of the corresponding gene USP39.

CONCLUSION

In conclusion, we explored histone lactylation in EC (Fig. S8) and found that lactate production in EC stimulated histone lactylation. In turn, histone lactylation regulated the expression of USP39, and USP39 activated the PI3K/AKT/HIF-1 α signaling pathway by interacting with PGK1. Finally, glycolysis was stimulated to produce more lactate, which further increased histone lactylation. Thus, histone lactylation may be a promising direction for research and a potential therapeutic target for EC.

Supplementary information

Additional file 1: Fig. S1. The modification levels of five lactylation sites in EC tissues and adjacent normal tissues. Fig. S2. IC50 of 2-DG and oxamate in Ishikawa and KLE cells. Fig. S3. The 2-DG and oxamate treatment suppresses migration, induces apoptosis, and arrests cell cycle progression of EC cells in vitro. Fig. S4. GO and KEGG enrichment analysis of differentially expressed genes from RNA-seq. Fig. S5. The analysis of TCGA database about USP39. Fig. S6. Images of HE staining for xenograft tumors and metastatic foci in the lung sections. Fig. S7. The image of silver staining to identify the interacting proteins. Fig. S8. Mechanism diagram.

METHODS

Cell culture

Five types of human EC cell lines (Ishikawa, RL95-2, HEC-1A, HEC-1B, and KLE) were obtained from the American Type Culture Collection (ATCC, USA). The normal endometrial cells we used were human primary endometrial epithelial cells. Cells were grown in DMEM/F12 complete medium (HyClone, China) supplemented with 10% fetal bovine serum (FBS; Gibco, USA) and penicillin and streptomycin (Booster, China) at final concentrations of 100 μ g/

mL. All cells were free from *Mycoplasma* contamination and were grown at 37 °C in a humidified atmosphere of 5% CO₂.

Clinical specimens

A total of 12 paired EC and adjacent normal tissues of patients who underwent surgery or biopsy at the Department of Gynecology, Union Hospital Affiliated to Tongji Medical College, Huazhong University of Science and Technology (Wuhan, China) from September 2019 to March 2021 were collected for immunohistochemistry (IHC) and western blot. All patients had complete clinical data and did not receive immunotherapy, chemotherapy, or radiotherapy. This study was approved by the Ethics Committee of Tongji Medical College, Huazhong University of Science and Technology (No. 2022-S017).

Bioinformatical analysis

TCGA (<http://www.cancergenome.nih.gov/>) was used for gene set enrichment analysis (GSEA) to analyze the expression and prognosis of USP39 in patients with EC. The ggplot2 package in R was applied to perform a volcano plot of all the differentially expressed genes based on the RNA-seq results.

Immunohistochemistry (IHC) staining and scoring

Samples were embedded in paraffin and sliced into sections at a thickness of 4 μm. The sections were then incubated with anti-L-lactyl lysine rabbit mAb (pan-anti-Kla; PTM-1401, PTM Bio, China), anti-lactyl-histone H3 (Lys18) rabbit mAb (anti-H3K18la; PTM-1406, PTM Bio, China), and anti-USP39 (23865-1-AP, Proteintech, China) at 4 °C overnight. The slides were then rinsed three times with PBS, incubated with a secondary antibody at room temperature for 30 min in the darkness, and visualized after being stained with a DAB solution. Three randomly selected fields were observed under a microscope (Motic, China). The IHC staining scores, based on the staining intensity (SI) and the percentage of immunoreactive cells (PR), were evaluated by two independent observers who were blinded to the patient's identity. The SI scores were assigned from 0 to 3 as follows: 0 = no staining; 1 = weak staining; 2 = moderate staining; and 3 = strong staining. The PR was scored from 1 to 4 as follows: 1 = 0–25%; 2 = 26–50%; 3 = 51–75%; and 4 = 76–100%. The PR and SI scores were multiplied to produce a weighted score for each patient. A score of 8–12 was defined as a high expression level, and a score of 0–7 was defined as a low expression.

Total RNA isolation and quantitative real-time polymerase chain reaction (qRT-PCR)

Adherent cells were harvested with the RNAiso reagent (Takara, Japan), and RNA was extracted according to the manufacturer's manual. The concentration of RNA was measured using a Tecan Infinite M200 Pro (Thermo Fisher Scientific, USA). cDNA was obtained from the RNA using a reverse transcription kit (Vazyme, China), and was used as a template for qRT-PCR with the SYBR Green Fast qPCR mix (ABclonal, China). The fold changes of RNA transcripts were calculated using the 2^{-ΔΔCt} method, and β-Actin was used as an endogenous control. All qRT-PCR runs were conducted in triplicate. The primer sequences used were as follows: USP39-F: 5'-GGTTGAAGTCTCACGCCTAC-3'; USP39-R: 5'-GGCAG-TAAACTTGAGGGTGT-3'; β-Actin-F: 5'-GGATTCCTATGTGGCGCAG-3'; and β-Actin-R: 5'-GATAGCACAGCCTGGATAGCA-3'.

Western blot

Fresh tissues or adherent cells were washed twice with PBS and then lysed on ice for 1 h with RIPA lysis buffer (Servicebio, China) containing a cocktail and PMSF. After centrifugation, total protein concentrations were determined using a BCA protein assay kit (Biosharp, China). Individual samples (20 μg/lane) were separated by sodium dodecyl sulfate (SDS)-polyacrylamide gel electrophoresis on 10–12% gels and transferred onto polyvinylidene difluoride membranes. After incubation with 5% dry milk in TBST at room temperature for 1 h, the membranes were washed and incubated with pan-anti-Kla (PTM-1401, PTM Bio, China), anti-H3K18la (PTM-1406, PTM Bio, China), anti-USP39 (23865-1-AP, Proteintech, China), anti-PGK1 (17811-1-AP, Proteintech, China), anti-PI3K (T40115, Abmart, China), anti-p-PI3K (T40116, Abmart, China), anti-AKT (T55561, Abmart, China), anti-p-AKT (T40067, Abmart, China), anti-HIF-1α (TA1009, Abmart, China), anti-β-Actin (AC038, ABclonal, China), and anti-H3 (17168-1-AP, Proteintech, China) at 4 °C overnight. After washing the membranes, the bound antibodies were detected with horseradish peroxidase-conjugated

secondary antibodies and visualized using an enhanced chemiluminescence (ECL) kit (Biosharp, China). The relative expression or modification levels of the targets to those of β-Actin or H3 were determined by densitometric analysis using the ImageJ software.

Glucose uptake, lactate accumulation, pyruvate content, and ATP content assays

EC cells were seeded into six-well plates and treated with 2-deoxy-D-glucose (2-DG), oxamate, or a plasmid for 24 h. Afterward, the cells were washed twice with PBS and lysed with a lysis buffer. The concentrations of glucose, lactate, pyruvate, and ATP were determined using commercial assay kits (S02015, Beyotime, China; A019-2-1, NJCIBIO, China; A081-1-1, NJCIBIO, China; A095-1-1, NJCIBIO, China), according to the manufacturer's instructions.

Half maximum inhibitory concentration (IC50) determination

3 × 10³ cells were seeded into 96-well plates and placed in the incubator for cell adhesion. According to the experimental settings, the drugs were adjusted to different concentrations and added 200 μL to each well. After treatment for 24 h, 100 μL serum-free medium containing 10% CCK-8 solution was added to each well and continued to incubate for 1 h. The absorbance of each well was measured at 450 nm and relative cell inhibition rates were calculated. After converting the drug concentration to log₁₀, the fitting curve was drawn to obtain the drug action concentration when inducing 50% cell death.

Cell counting kit-8 assay

Cell Counting Kit-8 (CCK-8; C0005, Targetmol, China) was used to measure cell proliferation. Cells were seeded into 96-well plates at a density of 3 × 10³ cells per well in a 100-μL suspension. Every 24 h for 5 days, 10 μL of the CCK-8 solution was added to each well in 100 μL of a serum-free medium. After incubation for 2 h at 37 °C, the absorbance of each well was measured at 450 nm using a microplate reader (Thermo Fisher Scientific, USA). Finally, the numbers of living cells over 5 days were plotted in a graph to reflect the cell proliferation rate.

Colony formation assay

For the colony formation assay, cells were seeded into six-well plates at a density of 1 × 10³ cells per well and cultured for 14 days. Subsequently, the cells were washed with PBS, fixed with 1 mL of methanol for 30 min, and stained with a crystal violet solution for approximately 30 min. After being washed and air dried, the colonies formed were counted manually.

5-Ethynyl-2'-deoxyuridine (EdU) assay

The EdU assay was performed with Ishikawa and KLE cells using an EdU-555 cell proliferation kit according to the manufacturer's protocol (C00755, Beyotime, China). Cells were seeded into six-well plates, and 24 h later, a 10 μM EdU solution was added to the cells for 2 h. Thereafter, the cells were fixed with 4% paraformaldehyde and rinsed three times with PBS and once with 0.5% Triton X-100. Next, a click additive reaction system was added to label the proliferated cells, and Hoechst 33342 was added for cell counting. Finally, cells were visualized using a fluorescence microscope (Olympus, Japan).

Cell migration assay

Transwell 24-well plates with an 8-μm pore size (Corning, USA) were used to assess cell migration. Endometrial cells were treated with histone lactylation inhibitors for 24 h firstly. Serum-free culture medium (100 μL) was added to the upper chamber with Ishikawa or KLE cells (1.0 × 10⁵/well), and 700 μL of a medium with 20% FBS as a chemo-attractant was placed into the lower compartment of the chamber. After 24 h incubation at 37 °C, cells that crossed the membrane were fixed with 4% paraformaldehyde (Servicebio, China) for 30 min and stained with 0.1% crystal violet (Servicebio, China) for 10 min at room temperature. Migrated cells were imaged and counted in three randomly selected fields of view using a CX23 light microscope (Olympus, Japan) with a 100× magnification.

Flow cytometry (FCM) analysis

An annexin V-FITC apoptosis detection kit (C1062M, Beyotime, China) was used to evaluate cell apoptosis, and a PI/RNase staining buffer (550825, BD Biosciences, USA) was used to analyze the cell cycle. The flow cytometer

used was an ID7000 spectral cell analyzer (Sony, Japan), and the data were analyzed using the FlowJo software.

Chromatin immunoprecipitation (ChIP)-qPCR

Ishikawa and KLE cells (3×10^6) were seeded into 100-mm dishes, and after treatment with 1% formaldehyde, the cells were lysed with 1 ml of RIPA lysis buffer. Genomic DNA was isolated and sheared into 200–400-bp fragments using a sonicator. After centrifugation, the supernatants were collected, and the chromatin was precipitated with anti-H3K18la (1:50; PTM-1406, PTM Bio, China) or IgG (30000-0-AP, Proteintech, China) at 4 °C overnight. The following steps were conducted according to the manufacturer's instructions for a ChIP assay kit (P2078, Beyotime, China). The primers designed for specific promoter regions of *USP39* are listed in Supplementary Table 1.

Electrophoretic mobility shift assay (EMSA)

Nuclear extracts were prepared from Ishikawa and KLE cells using a Nuclear and Cytoplasmic Protein Extraction Kit (P0027, Beyotime, China). The gel shift binding reaction was performed according to the instructions provided with the Chemiluminescent EMSA Kit (GS009, Beyotime, China). Samples were run on non-denaturing polyacrylamide gels and transferred to a Nylon membrane. After cross-linking, the biotin-labeled DNA was detected and visualized. Reduction in the mobility of DNA-protein complexes on the gels represented the binding of histone to the *USP39* promoter. The primer sequences of biotin-labeled probes were as follows: *USP39* c site: Bio-5'-AGCTGCGGCCCTCGGAGCAGCCCTGAAAGGTT-TAAAGGGCCGA-3' and *USP39* d site: Bio-5'-AAGTTGAGGTCCTAAGGCTT-GATGCCACACCAGCACCTGCGAG-3'.

Co-immunoprecipitation (Co-IP) assay and mass spectrometry (MS)

For immunoprecipitation (IP), cells were harvested and lysed with NP40 buffer (Servicebio, China), followed by the addition of PMSF and a protease inhibitor cocktail. After centrifugation, the supernatant was collected in fresh tubes. Approximately 1 mg of the cell lysate was incubated with 1.0 µg of primary antibodies (anti-IgG and anti-*USP39*) with a rotation overnight at 4 °C. Then, 25 µL of washed protein A agarose beads (HY-K0202, MCE, USA) were added to the lysate, and the incubation continued for 2 h at 4 °C with a rotation. Subsequently, the beads were collected by centrifugation and washed three times with NP40 buffer. The immune complex was released by boiling the beads with an SDS loading dye and analyzed by western blot. Purified peptides were picked up by autosampler and transferred into a C18 analytical column (Thermo Fisher Scientific, USA) for separation. A Q Exactive Plus mass spectrometer coupled with an EASY-nLC 1200 system (Thermo Fisher Scientific, USA) was used to acquire LC-MS/MS data and the MS raw data were analyzed with MaxQuant (V1.6.6) using the Andromeda database search algorithm, filtered with 1% FDR at both protein and peptide levels.

In vivo tumor formation

After random grouping into an experimental and control group, SPF BALB/c-nu female nude mice were subcutaneously injected with treated Ishikawa and normal Ishikawa cells (1×10^6), respectively. The tumor size was measured every 5 days, and then the mice were killed by cervical dislocation on day 25. The xenograft volume was calculated using the following formula: tumor volume (mm^3) = (length \times width²)/2. The tumors were weighed and embedded in paraffin for an IHC assay. Animal experiments were performed according to the protocols approved by the Animal Care and Use Committee of the Tongji Medical College (2021-S2783). For animal studies, the operation should obey blinding.

Mouse model of EC lung metastasis

After random grouping, SPF BALB/c-nu female nude mice were injected via the tail vein with Ishikawa cells (1×10^6 in 0.1 ml of PBS). After 6 weeks of treatment, the mice were killed by cervical dislocation. The lungs were excised, fixed, and embedded in paraffin to observe probable lung metastasis. For animal studies, the operation should obey blinding.

Statistical analysis

GraphPad Prism 8 (GraphPad Software, USA) was used for statistical analysis. Experimental data from three independent replicates are presented as the mean \pm standard deviation (SD). Student's *t* test was

used for comparisons between two independent sample groups with a normal distribution of data in qRT-PCR, Western blot, IHC scoring, colony formation assay, EdU assay, Transwell assay, glucose uptake assays, lactate accumulation assays, pyruvate content assays, ATP content assay, and flow cytometry analysis, et al. A one-way analysis of variance was used for group comparisons of all points in the curves when conducting CCK-8 assay and xenograft volume analysis. Overall survival curves were plotted via the Kaplan–Meier method and compared by the log-rank test. $P < 0.05$ was considered to indicate a statistically significant difference. * $P < 0.05$, ** $P < 0.01$, *** $P < 0.001$, **** $P < 0.0001$.

DATA AVAILABILITY

The raw data and materials supporting the conclusions of this article will be made available by the authors, without undue reservation.

REFERENCES

- Sung H, Ferlay J, Siegel RL, Laversanne M, Soerjomataram I, Jemal A, et al. Global Cancer Statistics 2020: GLOBOCAN estimates of incidence and mortality worldwide for 36 cancers in 185 countries. *CA Cancer J Clin.* 2021;71:209–49.
- Amant F, Moerman P, Neven P, Timmerman D, Van Limbergen E, Vergote I. Endometrial cancer. *Lancet.* 2005;366:491–505.
- Aoki Y, Kanao H, Wang X, Yunokawa M, Omatsu K, Fusegi A, et al. Adjuvant treatment of endometrial cancer today. *Jpn J Clin Oncol.* 2020;50:753–65.
- Paulino E, de Melo AC. Adjuvant treatment of endometrial cancer in molecular era: are we ready to move on? *Crit Rev Oncol Hematol.* 2020;153:103016.
- Siegel RL, Miller KD, Fuchs HE, Jemal A. Cancer statistics, 2022. *CA Cancer J Clin.* 2022;72:7–33.
- Hogg SJ, Beavis PA, Dawson MA, Johnstone RW. Targeting the epigenetic regulation of antitumour immunity. *Nat Rev Drug Discov.* 2020;19:776–800.
- Perri F, Longo F, Giuliano M, Sabbatino F, Favia G, Ionna F, et al. Epigenetic control of gene expression: potential implications for cancer treatment. *Crit Rev Oncol Hematol.* 2017;111:166–72.
- Biel M, Wascholowski V, Giannis A. Epigenetics—an epicenter of gene regulation: histones and histone-modifying enzymes. *Angew Chem Int Ed.* 2005;44:3186–216.
- Sabari BR, Zhang D, Allis CD, Zhao Y. Metabolic regulation of gene expression through histone acylations. *Nat Rev Mol Cell Biol.* 2017;18:90–101.
- Dawson MA, Kouzarides T. Cancer epigenetics: from mechanism to therapy. *Cell.* 2012;150:12–27.
- Verdin E, Ott M. 50 years of protein acetylation: from gene regulation to epigenetics, metabolism and beyond. *Nat Rev Mol Cell Biol.* 2015;16:258–64.
- Di Lorenzo A, Bedford MT. Histone arginine methylation. *FEBS Lett.* 2011;585:2024–31.
- Xie Z, Dai J, Dai L, Tan M, Cheng Z, Wu Y, et al. Lysine succinylation and lysine malonylation in histones. *Mol Cell Proteom.* 2012;11:100–7.
- Tan M, Peng C, Anderson KA, Chhoy P, Xie Z, Dai L, et al. Lysine glutarylation is a protein posttranslational modification regulated by SIRT5. *Cell Metab.* 2014;19:605–17.
- Tan M, Luo H, Lee S, Jin F, Yang JS, Montellier E, et al. Identification of 67 histone marks and histone lysine crotonylation as a new type of histone modification. *Cell.* 2011;146:1016–28.
- Xu H, Wu M, Ma X, Huang W, Xu Y. Function and mechanism of novel histone posttranslational modifications in health and disease. *Biomed Res Int.* 2021;2021:6635225.
- Ganapathy-Kanniappan S, Geschwind JF. Tumor glycolysis as a target for cancer therapy: progress and prospects. *Mol Cancer.* 2013;12:152.
- Koppenol WH, Bounds PL, Dang CV. Otto Warburg's contributions to current concepts of cancer metabolism. *Nat Rev Cancer.* 2011;11:325–37.
- Zhang D, Tang Z, Huang H, Zhou G, Cui C, Weng Y, et al. Metabolic regulation of gene expression by histone lactylation. *Nature.* 2019;574:575–80.
- Yu J, Chai P, Xie M, Ge S, Ruan J, Fan X, et al. Histone lactylation drives oncogenesis by facilitating m6A reader protein YTHDF2 expression in ocular melanoma. *Genome Biol.* 2021;22:85.
- Pan L, Feng F, Wu J, Fan S, Han J, Wang S, et al. Demethylzylasteral targets lactate by inhibiting histone lactylation to suppress the tumorigenicity of liver cancer stem cells. *Pharm Res.* 2022;181:106270.
- Jiang J, Huang D, Jiang Y, Hou J, Tian M, Li J, et al. Lactate modulates cellular metabolism through histone lactylation-mediated gene expression in non-small cell lung cancer. *Front Oncol.* 2021;11:647559.
- Yang J, Luo L, Zhao C, Li X, Wang Z, Zeng Z, et al. A positive feedback loop between inactive VHL-triggered histone lactylation and PDGFRβ signaling drives clear cell renal cell carcinoma progression. *Int J Biol Sci.* 2022;18:3470–83.

24. Arda Düz S, Mumcu A, Doğan B, Yılmaz E, İnci Coşkun E, Sarıdoğan E, et al. Metabolomic analysis of endometrial cancer by high-resolution magic angle spinning NMR spectroscopy. *Arch Gynecol Obstet*. 2022;306:2155–2166.
25. Troisi J, Sarno L, Landolfi A, Scala G, Martinelli P, Venturella R, et al. Metabolomic signature of endometrial cancer. *J Proteome Res*. 2018;17:804–12.
26. Pajak B, Siwiak E, Sołtyka M, Priebe A, Zieliński R, Fokt I, et al. 2-Deoxy-d-glucose and its analogs: from diagnostic to therapeutic agents. *Int J Mol Sci*. 2019;21:234.
27. Egger G, Liang G, Aparicio A, Jones PA. Epigenetics in human disease and prospects for epigenetic therapy. *Nature*. 2004;429:457–63.
28. Pavlova NN, Thompson CB. The emerging hallmarks of cancer metabolism. *Cell Metab*. 2016;23:27–47.
29. Martínez-Reyes I, Chandel NS. Acetyl-CoA-directed gene transcription in cancer cells. *Genes Dev*. 2018;32:463–5.
30. Lu SC. S-Adenosylmethionine. *Int J Biochem Cell Biol*. 2000;32:391–5.
31. Mills E, O'Neill LA. Succinate: a metabolic signal in inflammation. *Trends Cell Biol*. 2014;24:313–20.
32. Vaupel P, Schmidberger H, Mayer A. The Warburg effect: essential part of metabolic reprogramming and central contributor to cancer progression. *Int J Radiat Biol*. 2019;95:912–9.
33. Chen AN, Luo Y, Yang YH, Fu JT, Geng XM, Shi JP, et al. Lactylation, a novel metabolic reprogramming code: current status and prospects. *Front Immunol*. 2021;12:688910.
34. Brooks GA. Lactate as a fulcrum of metabolism. *Redox Biol*. 2020;35:101454.
35. Notarangelo G, Haigis MC. Sweet temptation: from sugar metabolism to gene regulation. *Immunity*. 2019;51:980–1.
36. Ippolito L, Morandi A, Giannoni E, Chiarugi P. Lactate: a metabolic driver in the tumour landscape. *Trends Biochem Sci*. 2019;44:153–66.
37. Wei R, Liu X, Yu W, Yang T, Cai W, Liu J, et al. Deubiquitinases in cancer. *Oncotarget*. 2015;6:12872–89.
38. Nijman SM, Luna-Vargas MP, Velds A, Brummelkamp TR, Dirac AM, Sixma TK, et al. A genomic and functional inventory of deubiquitinating enzymes. *Cell*. 2005;123:773–86.
39. Reyes-Turcu FE, Ventii KH, Wilkinson KD. Regulation and cellular roles of ubiquitin-specific deubiquitinating enzymes. *Annu Rev Biochem*. 2009;78:363–97.
40. Sanchez-Barcelo EJ, Mediavilla MD, Vriend J, Reiter RJ. Constitutive photomorphogenesis protein 1 (COP1) and COP9 signalosome, evolutionarily conserved photomorphogenic proteins as possible targets of melatonin. *J Pineal Res*. 2016;61:41–51.
41. Parsons JL, Dianova II, Khoronenkova SV, Edelmann MJ, Kessler BM, Dianov GL. USP47 is a deubiquitylating enzyme that regulates base excision repair by controlling steady-state levels of DNA polymerase β . *Mol Cell*. 2011;41:609–15.
42. Bingol B, Sheng M. Mechanisms of mitophagy: PINK1, Parkin, USP30 and beyond. *Free Radic Biol Med*. 2016;100:210–22.
43. Wu J, Chen Y, Geng G, Li L, Yin P, Newshean S, et al. USP39 regulates DNA damage response and chemo-radiation resistance by deubiquitinating and stabilizing CHK2. *Cancer Lett*. 2019;449:114–24.
44. Dong X, Liu Z, Zhang E, Zhang P, Wang Y, Hang J, et al. USP39 promotes tumorigenesis by stabilizing and deubiquitinating SP1 protein in hepatocellular carcinoma. *Cell Signal*. 2021;85:110068.
45. Pan XW, Xu D, Chen WJ, Chen JX, Chen WJ, Ye JQ, et al. USP39 promotes malignant proliferation and angiogenesis of renal cell carcinoma by inhibiting VEGF-A(165b) alternative splicing via regulating SRSF1 and SRPK1. *Cancer Cell Int*. 2021;21:486.
46. Noh KH, Kang TH, Kim JH, Pai SI, Lin KY, Hung CF, et al. Activation of Akt as a mechanism for tumor immune evasion. *Mol Ther*. 2009;17:439–47.
47. Semenza GL, Roth PH, Fang HM, Wang GL. Transcriptional regulation of genes encoding glycolytic enzymes by hypoxia-inducible factor 1. *J Biol Chem*. 1994;269:23757–63.
48. Fu D, He C, Wei J, Zhang Z, Luo Y, Tan H, et al. PGK1 is a potential survival biomarker and invasion promoter by regulating the HIF-1 α -mediated epithelial-mesenchymal transition process in breast cancer. *Cell Physiol Biochem*. 2018;51:2434–44.
49. Zhang Y, Cai H, Liao Y, Zhu Y, Wang F, Hou J. Activation of PGK1 under hypoxic conditions promotes glycolysis and increases stem cell-like properties and the epithelial-mesenchymal transition in oral squamous cell carcinoma cells via the AKT signalling pathway. *Int J Oncol*. 2020;57:743–55.
50. De Mello RA, Aguiar PN, Tadokoro H, Farias-Vieira TM, Castelo-Branco P, de Lima Lopes G, et al. MetaLanc9 as a novel biomarker for non-small cell lung cancer:

promising treatments via a PGK1-activated AKT/mTOR pathway. *J Thorac Dis*. 2018;10:52076–88.

ACKNOWLEDGEMENTS

We would like to thank Editage (www.editage.cn) for English language editing. We sincerely appreciate those who contributed to the publication of the article.

AUTHOR CONTRIBUTIONS

HW. designed and supervised the study. SW, JZ, and RZ conducted the experiments. RS, LA, ZY, and QZ analyzed data and prepared the initial manuscript. JZ, YY, and HL reviewed the manuscript. All authors read and approved the final manuscript.

FUNDING

This work is supported by the Major Technical Innovation Project in Hubei Province of China (Grant No. 2019ACA138), the National Key Research and Development Program of China (Grant No. SQ2018YFC010140), and the National Natural Science Foundation for the Youth of China (Grant No. 82002765).

COMPETING INTERESTS

The authors declare no competing interests.

CONSENT FOR PUBLICATION

All authors agree with the manuscript content.

ETHICS APPROVAL AND CONSENT TO PARTICIPATE

This study followed the ethical guidelines of the Declaration of Helsinki and was approved by the Ethics Committee of the Tongji Medical College of Huazhong University of Science and Technology (No. 2022-S017).

ADDITIONAL INFORMATION

Supplementary information The online version contains supplementary material available at <https://doi.org/10.1038/s41420-024-01898-4>.

Correspondence and requests for materials should be addressed to Hongbo Wang.

Reprints and permission information is available at <http://www.nature.com/reprints>

Publisher's note Springer Nature remains neutral with regard to jurisdictional claims in published maps and institutional affiliations.



Open Access This article is licensed under a Creative Commons Attribution 4.0 International License, which permits use, sharing, adaptation, distribution and reproduction in any medium or format, as long as you give appropriate credit to the original author(s) and the source, provide a link to the Creative Commons licence, and indicate if changes were made. The images or other third party material in this article are included in the article's Creative Commons licence, unless indicated otherwise in a credit line to the material. If material is not included in the article's Creative Commons licence and your intended use is not permitted by statutory regulation or exceeds the permitted use, you will need to obtain permission directly from the copyright holder. To view a copy of this licence, visit <http://creativecommons.org/licenses/by/4.0/>.

© The Author(s) 2024